Microscopic CO_2 Injection in Tight Rocks
Implications for Enhanced Oil Recovery and Carbon Geo-Storage

AlKharraa, Hamad; Wolf, Karl Heinz; AlQuraishi, Abdulrahman; Al Abdrabalnabi, Ridha; Mahmoud, Mohamed; Zitha, Pacelli

DOI
10.1021/acs.energyfuels.3c03403

Publication date
2023

Document Version
Final published version

Published in
Energy and Fuels

energy&fuels

Open Access

pubs.acs.org/EF

Article

Microscopic CO_2 Injection in Tight Rocks: Implications for Enhanced Oil Recovery and Carbon Geo-Storage

Hamad AlKharraa,* Karl-Heinz Wolf,* Abdulrahman AlQuraishi, Ridha Al Abdrabalnabi, Mohamed Mahmoud, and Pacelli Zitha*

Cite This: *Energy Fuels* 2023, 37, 19039–19052

Read Online

ACCESS | Metrics & More | Article Recommendations

ABSTRACT: Carbon dioxide (CO_2) injection has been widely used in conventional reservoirs for enhanced oil recovery and CO_2 sequestration. Nevertheless, the effectiveness of CO_2 injection in tight reservoirs is limited due to diagenetic processes that impact displacement efficiency. This research work assesses the performance of CO_2 injection in tight reservoirs and evaluates oil mobilization and fluid distribution within the rock pore systems. A set of experiments, including routine core analysis, X-ray diffraction (XRD), scanning electron microscopy (SEM), and mercury injection capillary pressure (MICP), was performed on Scioto sandstone. Three core-flooding runs were conducted to evaluate oil recovery of different injection schemes, including tertiary miscible CO_2 injection, secondary immiscible CO_2 injection, and secondary miscible CO_2 injection. A nuclear magnetic resonance (NMR) spectrometer was utilized to evaluate the fluid distribution in pre- and postflooding schemes. Results show that secondary miscible CO_2 injection provided the highest displacement efficiency (E_d) of 88%, with oil mobilized from both micro- and macropore systems, leading to the highest oil recovery of 93% original oil in place (OOIP). Tertiary miscible CO_2 injection had E_d of 67%, providing an ultimate oil recovery of 79% OOIP mostly from the macropore system. Limited contribution of micropores during the tertiary miscible CO_2 injection is attributed to the increased water content as a result of previously conducted secondary water flooding. Secondary immiscible CO_2 injection showed the least oil recovery among the injection schemes of 68% OOIP, which is attributed to the unstable displacement, as indicated by E_d of 52%. The efficiency of pore fluid displacement was determined through NMR analyses, and the findings are in line with the displacement efficiency values obtained from core-flood experiments, with a strong positive correlation. This finding is a promising strategy for determining a suitable CO_2 injection scheme in tight rocks for oil recovery and CO_2 storage.

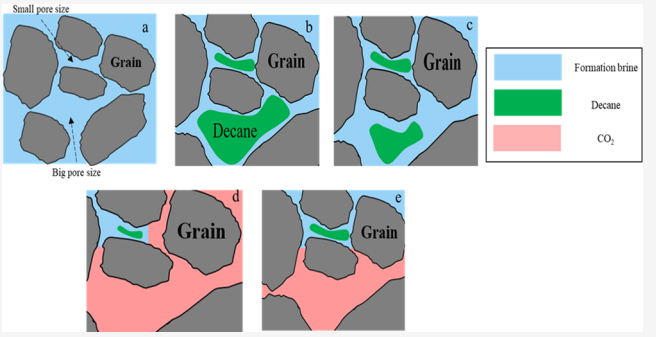

1. INTRODUCTION

Despite the world currently transitioning to renewable energy, oil remains the primary global energy source, contributing about 32% to the total energy sources, and it is expected to increase by around 6% in 2028.[1] This underlines the importance of improved and enhanced oil recovery (IOR/EOR) to increase oil production from both conventional and tight reservoirs to meet global oil demand. Conventional reservoirs are often characterized by high reservoir quality, producing oil using natural drive mechanisms.[2] As production continues, the natural drive mechanisms become insufficient to maintain the reservoir's energy, resulting in a lower oil recovery, typically less than 10% of the original-oil-in-place (OOIP).[3] Therefore, secondary methods are utilized by injecting water or gas to maintain pressure and hence increase oil recovery.[4] When oil recovery from secondary methods is insufficient, tertiary recovery or EOR is performed to sweep residual oil that cannot be targeted by secondary methods. EOR methods are categorized into thermal processes, such as steam injection and in situ combustion,[5] chemical methods, such as surfactant polymer and polymer flooding,[6] and miscible or immiscible gas injection, based on the type of gas injected, in situ oil, and reservoir conditions.[7]

Unlike the development plans of conventional reservoirs, tight rocks are characterized by low permeability (typically <1mD) and complex pore size distribution, covering both micro- and macropore systems. The complexity of pore systems can render fluid mobilization in tight rocks; therefore, attention is required

Received: September 6, 2023
Revised: November 1, 2023
Accepted: November 1, 2023
Published: November 17, 2023

Table 1. Summary of Main IOR/EOR Methods in Tight Reservoirs

recovery method	recovery mechanism	advantages	drawbacks	reference
multistage fracturing	frac fluid crack formation	increase in rocks' permeability	oil recovery <10%	9,10
	proppant keeps cracks open	increase in surface area	environmental hazards	
	pressure depletion	inexpensive		
water flooding	pressure support	wettability alteration	low injectivity	11−14
	oil displacement by water	inexpensive	oil recovery 15−38%	
			clay swelling	
immiscible CO_2 injection	partial gas dissolution	cost-effectiveness	poor microscopic displacement	17,18
	oil swelling expansion	pressure support		
miscible CO_2 injection	complete gas dissolution	high recovery >90%	requires high downhole pressure	19−22
	oil viscosity reduction	high displacement efficiency	high pressure (costly)	
	oil swelling expansion			

for selecting optimal recovery methods for economic production.[8]

Table 1 lists the main recovery methods utilized in the tight reservoirs. One commonly applied recovery method is multistage fracturing (MF), which is cost-effective compared to other recovery techniques.[9] However, MF shows low oil recovery (5−10% OOIP) due to low-pressure connectivity. In addition, the induced fractures might reach nearby water formations, resulting in high water production and environmental issues.[10] Waterflooding is a widely applied and economically feasible recovery method, with oil recovery ranging from 15 to 38% OOIP; however, it is not appropriate in tight reservoirs.[11] The low recovery using waterflooding in tight reservoirs is due to its low injectivity and small pore-throat sizes, which cause high capillary pressures, resulting in poor microscopic displacement efficiency (E_d).[12] E_d refers to

$$\frac{S_{oi} - S_{or}}{S_{oi}} \quad (1)$$

where S_{oi} represents the initial oil saturation and S_{or} represents the oil remaining in the rock.

Waterflooding can also cause clay swelling, reduction in permeability, and hence, recovery efficiency.[13] In addition, due to the difference in viscosity between displacing and displaced fluid, water channeling can lower volumetric sweep efficiency.[14] Gas flooding is the superior tertiary EOR choice because it reduces post-waterflooding residual oil. CO_2-EOR is a popular tertiary gas injection,[15] which has recently gained significant amounts of attention for its environmental benefits (i.e., CO_2 geo-storage).[16]

CO_2 is injected into a reservoir in miscible or immiscible modes. The immiscible injection is cost-effective compared to the miscible injection with CO_2 injected below the minimum miscibility pressure (MMP), at which CO_2 partially dissolves in the oil phase. However, this method can result in unfavorable mobility ratios, especially in tight reservoirs, leading to poor displacement efficiency.[17] Furthermore, the discrepancy in density between the injected CO_2 and the in situ oil promotes gravity override, reducing the amount of the recoverable oil.[18] Several studies indicate that miscible CO_2 injection provides higher oil recovery (typically >90% OOIP) than immiscible injection[19−21] due to significant reduction of interfacial tension, oil swelling, and oil viscosity reduction.[22]

Previous studies have revealed that injecting CO_2 is an effective approach for improving oil recovery in tight formations.[23−25]

Nevertheless, a knowledge gap exists regarding the performance of CO_2 injection in the micropore systems of tight reservoirs.

Tight rocks have complex pore systems, including micro- and macropores, due to depositional and diagenetic processes.[26] Macropores are voids between detrital grains, which form during the depositional process, while micropores originate before the depositional process and commonly exist between grains and authigenic clay minerals.[27] Compaction, the presence of quartz overgrowth, and small grain size can reduce the contribution of macropores in tight sandstones.[28,29] In contrast, clay coating prevents quartz overgrowth and thus preserves macropores.[30] Understanding these systems and their controlling factors is essential for selecting the optimal recovery method. A comprehensive study of petrographic and petrophysical analyses of different sandstones has been carried out to assess the contribution of the micropore system during CO_2-EOR and/or CO_2 sequestration,[31] which was based on routine core analysis, morphology, and mineralogy of different sandstones. The results indicate the presence of fibrous illite acting as pore bridging particles reducing the micropore throat system and hence lowering the microthroat modality ratio (MTMR), leading to a significant drop in microfluid content in tight sandstone samples. MTMR is a dimensionless number that relates the microthroat size to the macrothroat size in sandstone rocks. A large MTMR reveals that most of the displacing fluid primarily flows into the macropore throat (following the least resistance paths), avoiding the micropore throat system, resulting in low overall fluid displacement. However, the absence of fibrous illite and the presence of illite platelets lead to high MTMR due to the clear preservation of the micropore throat system. In addition, the higher the microthroat contribution in the overall pore system is, the more confined is the micropore system.[32] Accordingly, Scioto sandstone was selected to represent the complexity of marginal (tight) reservoirs. This study aims to explore the effectiveness of CO_2 injection in tight rocks and assess the displacement contribution of micro and macropore fluids at different injection modes (miscible and immiscible, both at secondary and tertiary injection modes). CO_2 injection was examined using core-flooding and nuclear magnetic resonance (NMR) measurements before and after core-flood tests to evaluate pore fluid distributions at each saturation condition.

2. MATERIALS, EXPERIMENTAL SETUPS, AND PROCEDURE

2.1. Materials. Scioto sandstone cores were used in this study to represent tight sandstone formations. Core samples were obtained from

https://doi.org/10.1021/acs.energyfuels.3c03403
Energy Fuels 2023, 37, 19039−19052

the Buena Vista member near McDermott, Southern Scioto County, Ohio.[33] Scioto sandstone is often used in laboratory studies to model tight sandstones due to its homogeneous characteristics, which are suitable for comparable petroleum engineering laboratory tests.[34]

A set of cylindrical plugs measuring 3.8 cm in diameter and 8.0 cm in length underwent a 48 h drying and vacuuming process at 75 °C.

Subsequently, plugs of 5 cm in length were cut for porosity and permeability, NMR T_2, and core-flooding experiments. The remaining samples were utilized for the XRD, SEM, and MICP tests. The average gas porosity and permeability were determined using a helium porosimeter and nitrogen gas permeameter, and the values are 17.5 vol % and 1.2 mD, respectively. Nine core plugs were selected to compose three sets of composite cores made of three plugs, each to be used in this study. Plugs were lined up face to face in a horizontal manner in a heated shrinkable Teflon tape sleeve to prevent end-capillary effects.[35] Three composites of 3.8 cm in diameter and 15 cm in length were used in the core-flooding experiments. Table 2 lists the petrophysical properties of the composites used in this study.

Table 2. Properties of the Scioto Sandstone Composites[a]

composite ID	core plugs ID	pore volume (cc)	porosity (vol %)	permeability (mD)
1	S22, S23, S25	30.48	18.45	1.21
2	S12, S13, S14	31.04	18.53	1.24
3	S34, S35, S24	30.96	18.82	1.20

[a]The estimated petrophysical properties are the average of the plugs' values.

Synthetic formation brine was used to represent the connate water saturation, and synthetic seawater brine was used as the displacing phase during waterflooding injection. Synthetic formation brine was prepared by mixing salts with distilled water to resemble the local formation brines. Synthetic seawater brine was formulated according to the Arabian Gulf seawater composition and salinity.[36] The compositions and salinities of both brines are presented in Tables 3 and 4, respectively.

Table 3. Constitutes of Synthetic Formation Water (Total Dissolved Solids = 236,840 mg/L)

component	formation water (mg/L)
sodium chloride	148,750
calcium chloride	69,400
magnesium chloride	17,910
sodium sulfate	390
sodium bicarbonate	390

n-Decane (*n*-C_{10}) was used to represent the oleic phase, and this choice was made to avoid rock wettability alteration.[37] Several studies have reported that the MMP of decane and CO_2 is around 85 bar (1235 psi) at 40 °C.[38,39] Therefore, miscible flooding runs were conducted at a higher injection pressure of 124 bar (1,800 psi) to ensure good miscibility. Oil density and viscosity were measured using an Anton Paar-DMA 4500M density meter and an Oswald viscometer, respectively. Pure carbon dioxide (CO_2) (99.9%) was utilized as the gaseous phase. Table 5 lists the physical properties of the fluids under the experimental conditions.

Table 5. Fluid Physical Properties Measured under Experimental Conditions at 124 bar and 40 °C

fluid	density (g/cm^3)	viscosity (cP)
formation water	1.133	1.21
seawater	1.025	1.10
decane	0.730	0.89
sc-CO_2[a]	0.644	0.05

[a]CO_2 properties were obtained from the National Institute for Standards and Technology (NIST) Web-book.[40]

2.2. Experimental Setups. A Core-Lab gas permeameter was utilized to determine gas and Klinkenberg liquid permeabilities, and the volumetric method was used to estimate the plug's porosity. XRD was conducted on crushed samples to determine the mineral and elemental compositions using a Rigaku ULTIMA IV X-ray diffractometer with CuKα radiation at 40 kV and 40 mA with a 2θ range of 3−100° at 0.02° step size within an 8 min period. XRD patterns were then analyzed by using X'Pert High Score Software.

SEM analyses were conducted on thin chips utilizing a TESCAN instrument (model MIRA3) coupled with an EDX detector to generate SEM density images with a pixel resolution in nanometers to identify micropores and clay morphologies. NMR T_2 measurements were performed on core plug pre- and postflood experiments to evaluate the pore fluid distribution at different fluid saturations. These measurements were taken using a resonating frequency of 2 MHz at an ambient temperature via an NMR spectrometer from the Oxford Core Analyzer GeoSpec 2-75. The Carr−Purcell−Meiboom−Gill (CPMG) pulse sequence was used to generate magnetization decay with an echo spacing of 110 μs and a signal-to-noise ratio of 150 SNR. The decaying magnetization was converted to T_2 distributions using Green Imaging Technologies (v6.1) software from Oxford Instruments.[41]

A Micrometrics Auto Pore V 9600 instrument was utilized for mercury intrusion capillary pressure (MICP) analysis. The MICP experiment was conducted on a representative dry cylindrical 1.27 cm-long and 1.27 cm-diameter plug to estimate throat size distribution within the range of 0.003−500 μm at incremental injection pressures up to 60,000 psi (450 MPa). A centrifuge at 18,000 rpm was utilized to desaturate the core samples to connate water saturation with *n*-decane as the displacing phase. Flooding runs were conducted using a flooding unit (Figure 1). The unit consists of an injection pump, core holder, and production collection system connected through 1/8 in. stainless steel tubes with multiple air pneumatic two- and three-way valves to control fluid direction. The core holder is a Hassler-type core holder capable of housing samples of 1.5 in. (3.8 cm) in diameter with a length of up to 12 in. (30.5 cm). Two inline pressure transducers are utilized to measure the pressure drop across the core sample ends with ±0.05% full-scale pressure accuracy. The fluid injection system is made of a DCI dual syringe pump displacing distilled water at desired injection rates with a precision of 0.001 cc/min to the bottom of three 1 L Hastelloy floating piston accumulators. The accumulators were used to house *n*-decane, CO_2 gas, and seawater. A dome-type back pressure regulator (BPR) connected to the production end of the core holder was used to control and maintain the desired pore pressure up to 6000 psi. The setup components were housed within an oven for temperature control up to 150 ± 0.1 °C. The flooding unit can operate at a confining pressure of up to 10,000 psi. All the components are linked to a control system and data logger connected to a personal computer for experiment control and online data gathering. A gas booster was used to pressurize the CO_2 accumulator. The production collection system consists of graduated tubes placed in a timely set of fraction collectors to collect liquid effluents.

Table 4. Constitutes of Synthetic Seawater (Total Dissolved Solids = 68,602 mg/L)

total alkalinity (mg/L)	bicarbonate (mg/L)	calcium (mg/L)	magnesium (mg/L)	sodium (mg/L)	potassium (mg/L)	chloride (mg/L)	sulfate (mg/L)	nitrate (mg/L)	fluoride (mg/L)
174	212	766	2648	22,353	810	36,585	5015	37	2.19

https://doi.org/10.1021/acs.energyfuels.3c03403
Energy Fuels 2023, 37, 19039−19052

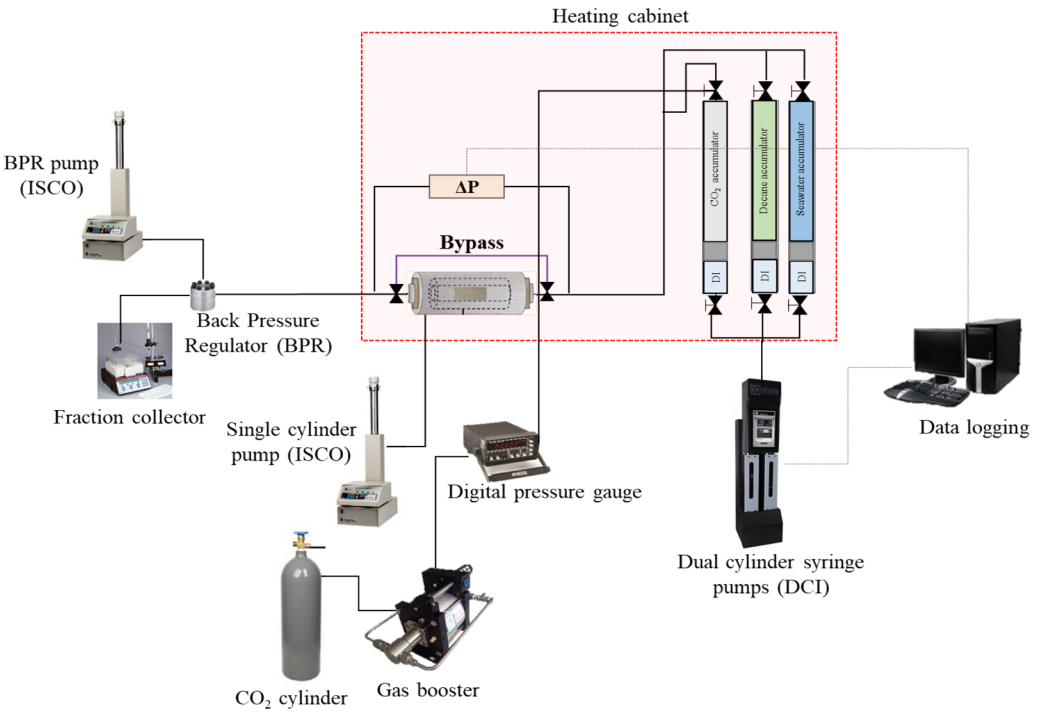

Figure 1. Schematic of the experimental setup used for core-flood experiments.

2.3. Experimental Procedures. The core samples were characterized by using XRD, SEM, MICP, and routine core analysis (RCA) measurements. Experimental work was started by determining the pore morphology analysis of Scioto sandstone by using SEM imaging. MICP was then performed on representative consolidated plugs to estimate the rock pore-throat distribution. Nine dry samples with a radius of 3.8 cm and a length of 5 cm were used to measure the average values of porosity and Klinkenberg liquid permeability using a Vinci helium porosimeter and Core-Lab gas permeameter, respectively. The dry samples were saturated with formation brine, utilizing a saturation unit under a pressure of 2000 psi to ensure complete saturation. The plug's porosity was redetermined by using the mass balance method. Then, NMR T_2 measurements were taken on these brine-saturated plugs to identify the NMR pore fluid distribution (PFD). A centrifuge was utilized to desaturate the brine-saturated samples with *n*-decane as the displacing phase; hence, OOIP and connate water saturation were determined. These samples were subsequently subjected to NMR T_2 measurements to calculate the movable and bound fluids. Three composite cores of three core plugs each were assembled, and three flooding runs were performed with different fluid injection schemes. These runs are tertiary miscible CO_2 injection (Experiment 1), secondary miscible CO_2 injection (Experiment 2), and secondary immiscible CO_2 injection (Experiment 3). Table 6 presents the description and conditions of the core-flood experiments. All runs were conducted at 0.2 cc/min injection rate and a constant temperature of 40 °C. Waterflooding was started into the first composite core at connate water saturation, and injection continued until oil production ceased after 3.5 PV of seawater injection. Subsequently, tertiary miscible CO_2 was injected with a total of 3.8 PV of CO_2 injection. In the second run, secondary miscible CO_2 injection was conducted using the second composite core at connate water saturation with an injection of 3.5 PV. Immiscible CO_2 was performed in the third composite core, at connate water saturation, for 7.2 PV of CO_2 gas injection. The *n*-decane produced in all experiments was collected and corrected by deducting the inlet and outlet dead volumes. Differential pressures were continuously measured and recorded throughout the injection runs. At the end of each experiment, the oil recovery, displacement efficiency, and injectivity index were evaluated. NMR T_2 measurements were aging-performed at the end of each run to determine the final fluid distribution and verify the calculated resident fluid volumes determined by material balance.

Table 6. Three Core-Flood Experiments Were Performed on Three Composites at an Average Connate Water Saturation of 32% and an Average Initial Oil Saturation of 68%

run no.	experiment description	confining pressure (psi)	pore pressure (psi)	pore volume injected (%PV)
1	waterflooding + miscible CO_2	2500	1800	7.3
2	only miscible CO_2 injection	2500	1800	3.5
3	only immiscible CO_2 injection	1700	1400	7.2

3. RESULTS

An integrated approach was implemented to assess the impact of injection schemes on tight rocks and evaluate the role of these injection modes on the micropore system displacement in tight sandstones. This section presents a detailed description of the experimental results obtained and their analyses.

3.1. Mineralogy, Morphology, and Petrophysical Properties. XRD results reveal that Scioto sandstone is relatively clean sand (high quartz content of 89.2%), associated with small amounts of feldspar and clay minerals of 2.8 and 4.1%, respectively (Table 7).

The measured average permeability of Scioto sandstone was measured to be 1.21 mD. Some researchers have categorized tight reservoirs by permeability lower than 0.1 mD[32] (Figure 2); however, classifying the rock based on a definite threshold value could lead to an unsuitable EOR technique that causes poor fluid displacement.

Although Scioto's permeability is greater than 0.1 mD, MICP reveals that Scioto has a narrow pore-throat distribution ranging from nanometers to approximately 2.4 μm (Figure 3). Based on the pore system characterization by Nelson,[42] the Scioto

https://doi.org/10.1021/acs.energyfuels.3c03403
Energy Fuels 2023, 37, 19039−19052

Table 7. Mineralogical Compositions of Scioto Sandstone (Units in wt %)

sample	quartz	plagioclase	orthoclase	anhydrite	ilmenite	siderite	dolomite	halite	hematite	pyrite	chlorite	illite	kaolinite
Scioto	89.2	2.1	0.7	3	0	0.2	0	0.2	0.5	0	0.9	2.2	1

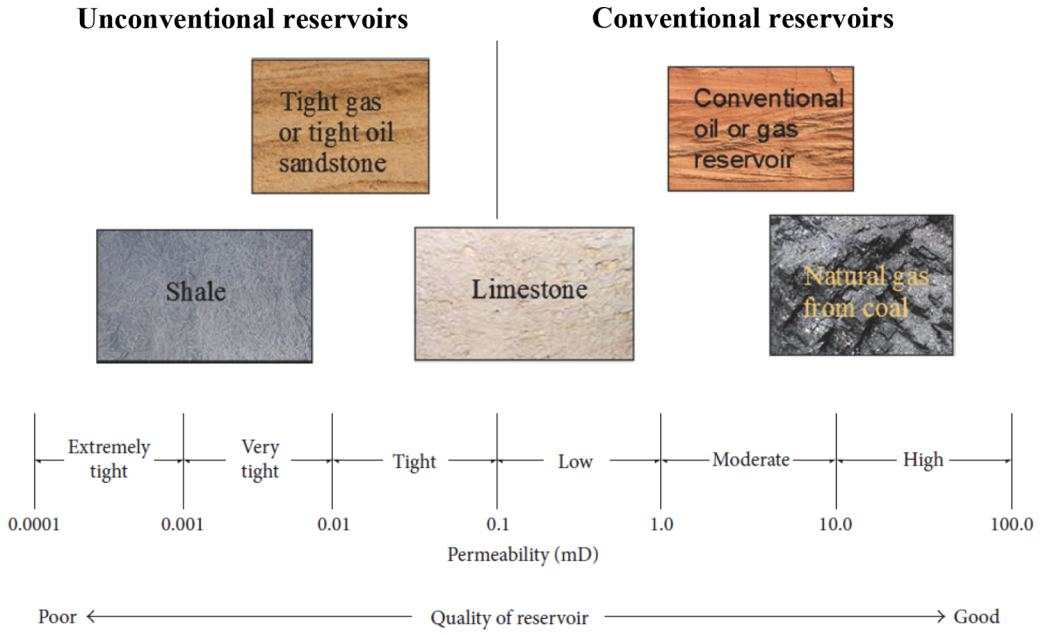

Figure 2. Classification of unconventional reservoirs using the permeability threshold, $k < 0.1$ mD. Adapted with permission from ref 32. Copyright 2017 Geofluids.

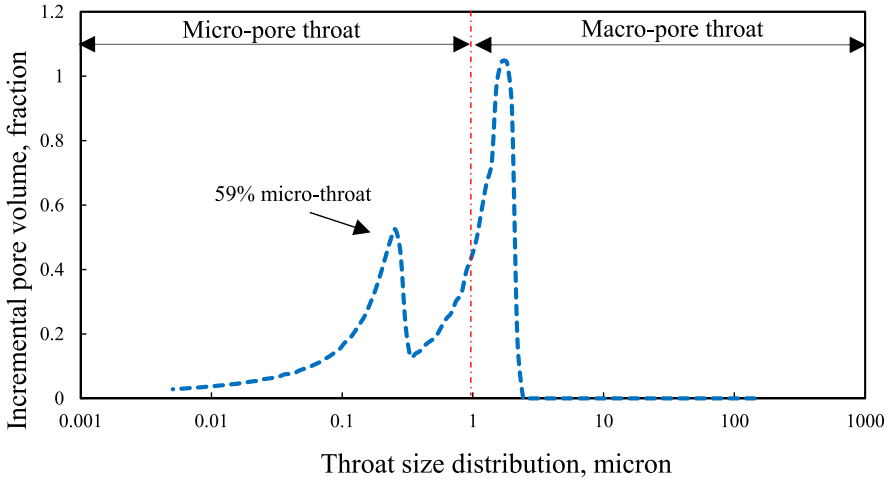

Figure 3. Pore-throat distributions of Scioto sandstone were obtained using MICP.

micropore throat makes up approximately 59% of the total pore throat system.

The SEM of Scioto sandstone indicates a clear micropore throat proportion that can be attributed to the absence of fibrous illite and illite platelets (Figure 4). The MTMR, a dimensionless number that relates the abundance size of the micropore throat to the macropore throat, can be used to evaluate the pore fluid displacement efficiency of the EOR methods. Scioto sandstone has 1.44 MTMR, implying that an efficient EOR method should be carefully considered to enhance fluid displacement across different pore sizes and prevent oil bypassing caused by high capillary pressure.

3.2. Core-Flooding Results. Three flooding runs were conducted by using three composite cores of Scioto sandstone. This section presents the main results of the performed runs, including the ultimate oil recoveries, pressure drop profiles, injectivity indices, and corresponding displacement efficiency calculations (Table 8). OOIP of the composite core represents the sum of oil volumes for each core. E_d refers to the ratio of mobilized oil to OOIP, and it can be calculated as follows:

$$\frac{S_{oi} - S_{or}}{S_{oi}} \tag{2}$$

where S_{oi} represents the initial oil saturation and S_{or} represents the oil remaining in the rock.

In the first run, waterflooding was performed in secondary injection mode, followed by miscible tertiary CO_2 injection. Figure 5 presents the oil recovery and pressure drop profiles of

https://doi.org/10.1021/acs.energyfuels.3c03403
Energy Fuels 2023, 37, 19039−19052

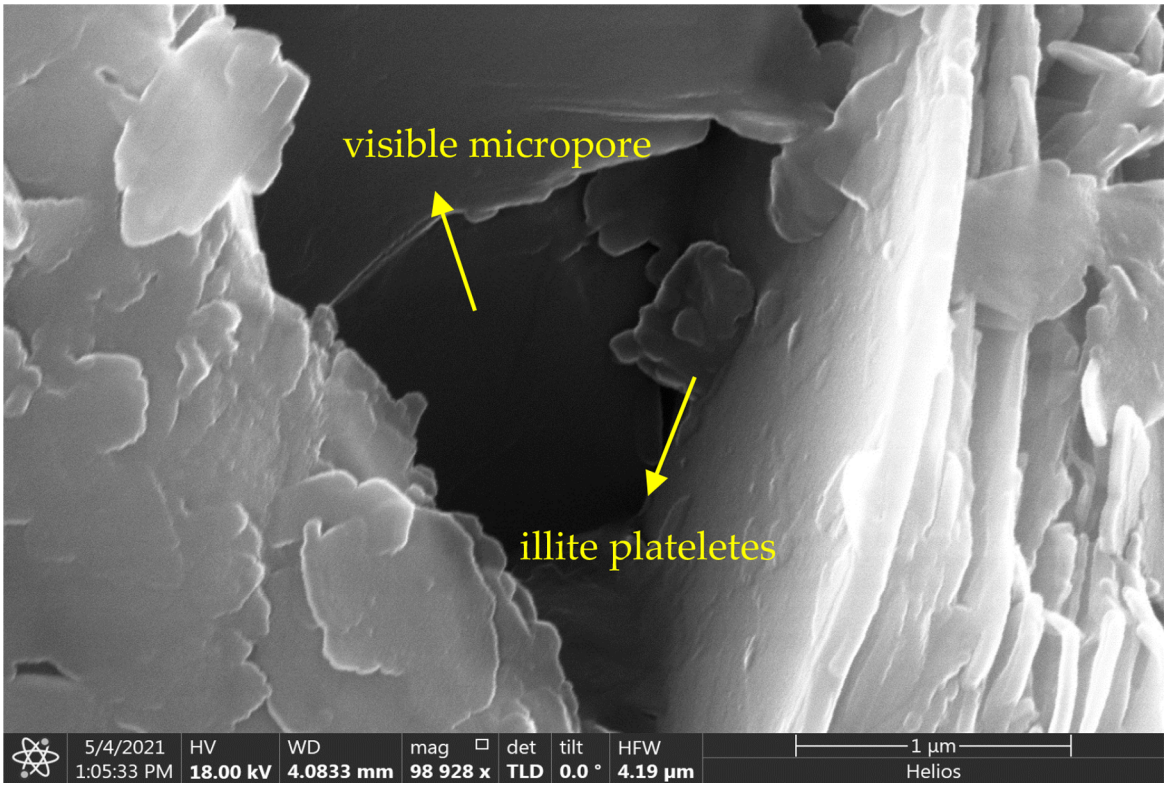

Figure 4. SEM micrographs showing pore-lining illite and clear micropore.

Table 8. Comparison of the Ultimate Oil Recovery, Displacement Efficiency, and Injectivity Index

run no.	ultimate recovery (% OOIP)	displacement efficiency (%)	injectivity index (cc/min/psi)
1	79	60	0.01
2	93	88	0.16
3	68	52	0.08

this run along the injected pore volume. Oil recovery using secondary waterflooding 35% OOIP, and an additional 44% OOIP oil recovery was obtained using tertiary miscible CO_2 injection.

The pressure drop increased sharply throughout the experiment to a maximum pressure value of about 160 psi (11 bar) due to the mobility difference between the wetting and nonwetting fluid in the large pores, leading to oil recovery of 31% OOIP at approximately 0.23 PV of seawater injection, where a water breakthrough was observed.

The pressure drop decreased slowly afterward to constant values that ranged around 124 psi (8.5 bar) due to seawater dominating the fluid flow and diminishing oil displacement within the pore system at 3.6 PV. The relatively poor recovery using waterflooding could be attributed to the viscosity difference between injected brine and displaced *n*-decane, which led to viscosity fingering and high capillary pressure in

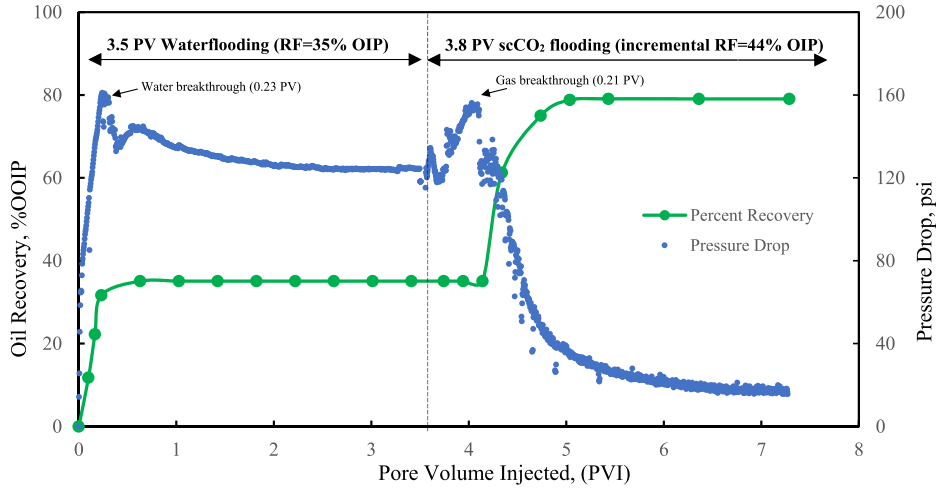

Figure 5. Oil recovery and pressure drop of secondary water flooding followed by miscible tertiary CO_2 injection conducted on composite #1.

https://doi.org/10.1021/acs.energyfuels.3c03403
Energy Fuels 2023, 37, 19039−19052

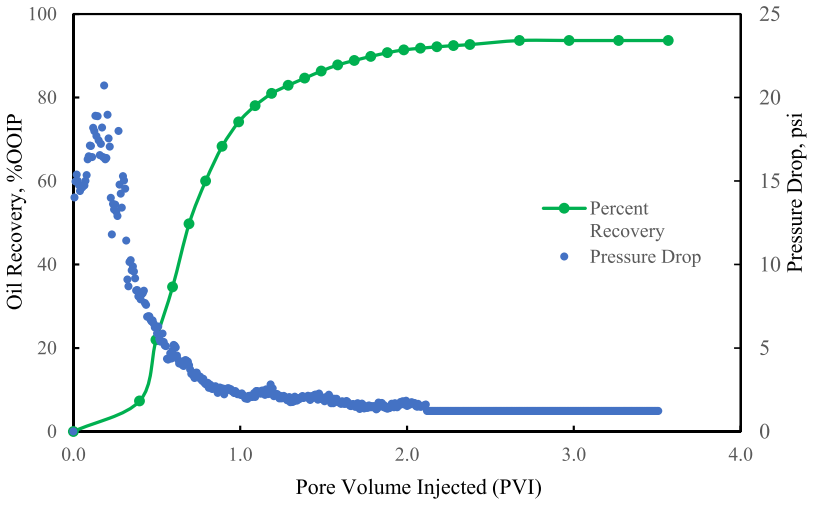

Figure 6. Oil recovery and pressure drop of miscible secondary CO_2 injection conducted on composite core #2.

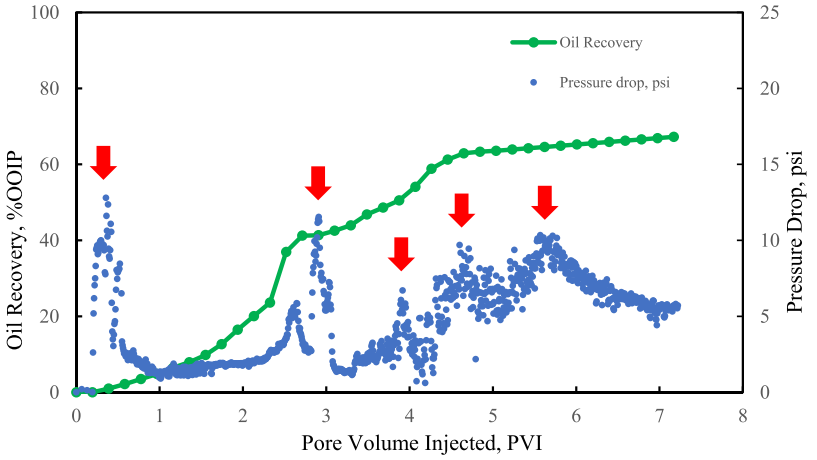

Figure 7. Oil recovery and pressure drop of immiscible secondary CO_2 injection conducted on composite core #3.

tiny pores. Subsequently, a tertiary miscible CO_2 injection was started, and the pressure drop profile builds to a peak value of around 155 psi (10.6 bar) as a result of CO_2 attempting to overcome the water pressure residing in the pores after waterflooding. The gas breakthrough occurred at around 0.21 PV of gas injection, followed by a significant reduction in pressure drop to about 16 psi (approximately an 89% drop from its maximum value). The experiment was terminated after a total injection of 7.3 PV, and the estimated displacement efficiency and injectivity index at the end of the experiment are 67% and 0.01 cc/min/psi, respectively. We presume that the low injectivity of miscible tertiary CO_2 is due to excessive water imbibing the pores prior to CO_2 flooding. This finding aligns well with that of Blunt et al.,[43] who reported that postwaterflooding residual oil exhibits high capillary pressure. The second run performed on composite no. 2 was secondary miscible CO_2 injection conducted at connate water saturation. Oil recovery and pressure drop profiles are listed in Figure 6. In this run, the pressure drop profile increases to around 23 psi with oil recovery starting at 0.3 PV of miscible gas injection. The recovery profile continuously increases to a maximum of 93% OOIP, and the pressure profile falls to around 5 psi. The total CO_2 injection was terminated after approximately 3.5 PV of gas injection when the oil recovery ceases. High oil recovery using miscible CO_2 injection is attributed to the high injectivity of 0.16 cc/min/psi and the CO_2-decane phase miscibility achieved, which yields a stable displacement efficiency of 88% compared to the previous injection schemes.

The third run was an immiscible secondary CO_2 injection conducted in composite #3. The oil recovery and pressure drop profiles are presented in Figure 7. In this run, oil recovery started at 0.38 PV after immiscible gas injection. The delay in production is attributed to unfavorable displacement caused by gas channeling due to the density difference between CO_2 gas and *n*-decane.[44] Based on the fluctuation in the pressure drop profile marked in red arrows, CO_2 injection seems to be unstable, resulting in a low displacement efficiency of 52% after a total immiscible CO_2 injection of 7.2 PV. The oil recovery profile continues to increase due to CO_2 injection; however, the recovery process was slow, as expected,[45] and thus, the experiment was terminated. The ultimate oil recovery was the lowest among the injection schemes tested, resulting in 67% OOIP.

3.3. NMR T_2 Measurements. The incremental T_2 relaxation is proportional to pore size distribution.[46] Macropores have longer T_2 values, whereas micropores tend to have shorter T_2 values; hence, the pore volumes of various pores can be analyzed.[47] NMR T_2 measurements were performed before and after the flooding process in all experiments to investigate the pore fluid distribution in tight rocks. Figure 8 depicts NMR T_2

https://doi.org/10.1021/acs.energyfuels.3c03403
Energy Fuels 2023, 37, 19039−19052

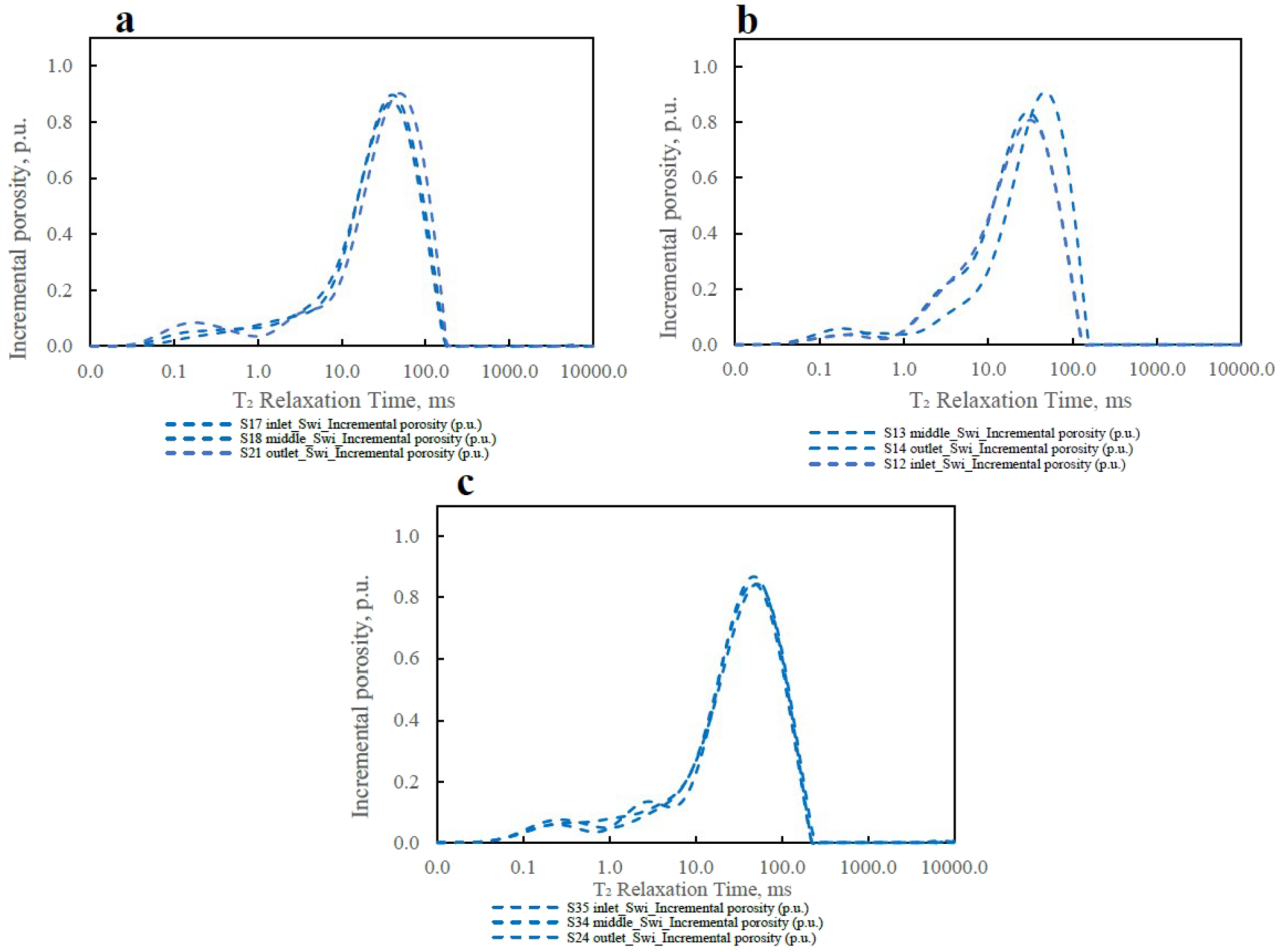

Figure 8. Incremental NMR T_2 measurements of brine-saturated composites of Scioto sandstone: (a) Composite 1, (b) Composite 2, and (c) Composite 3.

measurements of the three brine-saturated plugs forming the three composites. Clearly, profiles show identical unimodal characteristics, with T_2 values ranging from 0.1 to 177 ms.

Brine-saturated plugs of the tested composites were desaturated to connate water saturation with *n*-decane at 18,000 rpm. Figure 9 presents the NMR profiles at the end of the desaturation process. Connate water resides in the micropores, resulting in shorter T_2 relaxation values, while *n*-decane moves to the macropores and consequently reveals longer T_2 relaxation values.

Hence, NMR T_2 measurements reveal two signals,[48] and the results obtained agree with this and show two signals: the left signal with shorter T_2 values ranging from 0.1 to 39 ms, representing micropores primarily containing irreducible water, and the right signal with longer T_2 values ranging from 79 to 892 ms, referring to macropores in which *n*-decane resides.

It is worth noting that desaturated composite signals show extended T_2 relaxation values (right signal) compared to those of brine-saturated spectra. This is because of the wettability effect that delays T_2 relaxation and causes longer T_2 values.[49] The T_2 cutoff value is utilized to determine the fluid residing in the micro- and macropore pores of composite sandstones. The results demonstrate that the T_2 cutoff value of the Scioto sandstone is 24.6 ± 1.3 ms, which is consistent with the literature findings.[50,51] The findings indicate that the prepared composites comprise an average of 65% macropores and 35% micropores.

Figure 10 depicts the composite cores' incremental NMR T_2 relaxation time before (desaturated condition) and after CO_2 injection to diagnose the effect of CO_2 injection on pore fluid displacement in tight rocks. As mentioned earlier, the area under the incremental T_2 curve of the desaturated state represents the amount of hydrogen in the pore system. A reduction in this area indicates a lack of hydrogen caused by the CO_2 injection and the consequent production of fluid from the given pores. For the miscible tertiary CO_2 injection, the incremental post-CO_2 injection NMR T_2 curve (Figure 10a) shows a unimodal distribution ranging from 0.1 to approximately 50 ms. The macropore signal of the desaturated composite core clearly vanished due to the displacement of CO_2 (marked with a blue arrow in Figure 10a). No apparent reduction was seen in the left signal of the desaturated state (micropores), indicating that injected CO_2 could not reach the tiny pores (marked with a black arrow in Figure 10a). In addition, the micropore signal was observed to exhibit a slight increase of around 9% compared to the originally observed signal pre-CO_2 injection, which is believed to be due to the increase in water content after the secondary water injection prior to tertiary CO_2 injection. The incremental T_2 spectrum at the end of the secondary miscible CO_2 injection of composite core #2 illustrates a unimodal signal ranging from 0.1 to 22.4 ms (Figure 10b). The narrower range of T_2 values compared to composite core #1 (tertiary miscible CO_2 injection) corresponds to fluid displacement from small pores. The micropore signal had a clear reduction of approximately

https://doi.org/10.1021/acs.energyfuels.3c03403
Energy Fuels 2023, 37, 19039−19052

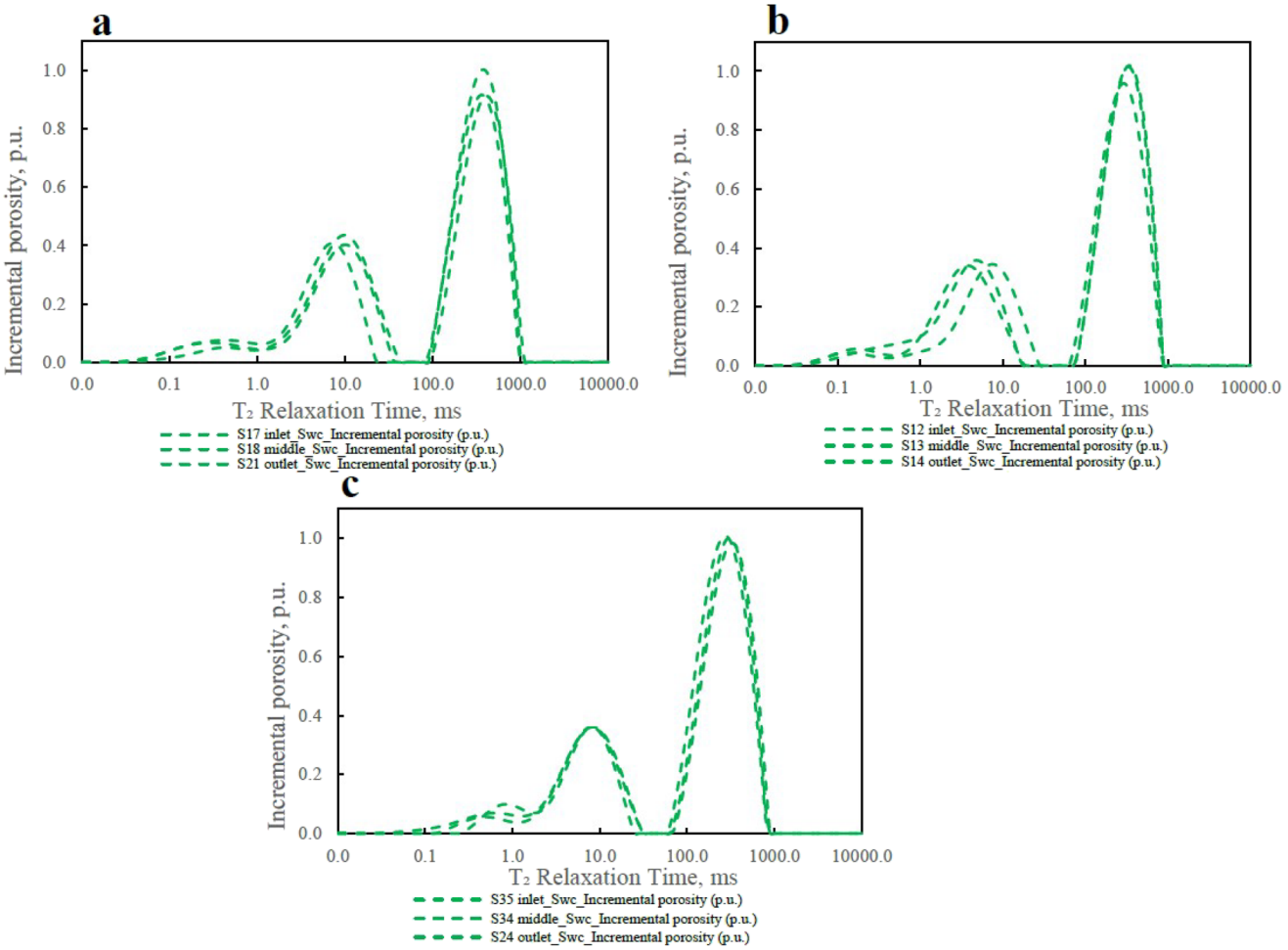

Figure 9. Incremental NMR T_2 measurements of desaturation for Scioto sandstone: (a) Composite 1, (b) Composite 2, and (c) Composite 3.

12% compared with the initial desaturated state, indicating that CO_2 injection was able to invade the micropore system (marked with a black arrow). Furthermore, secondary miscible CO_2 injection ultimately eliminated the macropore signal (marked with a blue arrow). Figure 10c presents the incremental T_2 distributions of an immiscible secondary CO_2 injection. The profile shows broader T_2 distributions ranging from 0.1 to almost 560 ms, indicating that hydrogen molecules are still within the micro- and macropore systems, and immiscible secondary CO_2 injection shows poor resident fluid mobilization. The NMR technique was used to estimate the displacement efficiency (ED_{NMR}) and evaluate pore fluid reduction. ED_{NMR} is the ratio of change in incremental T_2 profiles under desaturated and post-CO_2 injection conditions to NMR at the initial desaturated state. ED_{NMR} for the three injection schemes demonstrated that secondary miscible CO_2 flooding provided the highest value of approximately 70%, followed by tertiary miscible CO_2 flooding at around 55% and finally secondary immiscible CO_2 injection, which showed the lowest value of 47% (Table 9).

Table 10 and Figure 11 present the results of NMR displacement efficiency in NMR micro- and macropore signals due to fluid deficiency. The results show that the NMR displacement efficiency in macropores using tertiary and secondary miscible CO_2 injections provides significant reductions of 94 and 100%, respectively. Secondary immiscible CO_2 injection shows the least macropore displacement efficiency, with 67%. It also reveals no clear micropore reduction compared to that observed originally at desaturated state due to unstable displacement. On the contrary, the micropore signal of secondary miscible CO_2 injection showed a 12% reduction in contrast to tertiary miscible CO_2 injection that demonstrated no significant change in micropores signal.

4. DISCUSSION

Petrophysical results revealed that Scioto sandstone has a relatively wider pore-throat size distribution covering micro- and macropore throat systems with an estimated average throat diameter of 1.8 μm, indicating the presence of a tight microthroat system. Mineralogy and elemental analyses reveal that Scioto has a low total clay content of 4.1% composed of illite, kaolinite, and chlorite. SEM results also demonstrate that illite platelets lead to a clear preservation of Scioto's micropore throat, attributing to 59.1% of the total pore-throat system. The calculations show that Scioto has high MTMR, and we hypothesized earlier that rock with a high modality ratio requires a suitable recovery method to obtain stable and efficient displacement in tight rocks. Core-flood results show that secondary waterflooding is not an optimal recovery process in tight rock. This is attributed to the early water breakthrough. We deduce that most of the oil recovery is produced from macropores, as water follows pathways of least resistance bypassing the micropore system.[52] This low oil recovery can also be attributed to the low water injectivity index of 0.002 cc/min/

https://doi.org/10.1021/acs.energyfuels.3c03403
Energy Fuels 2023, 37, 19039−19052

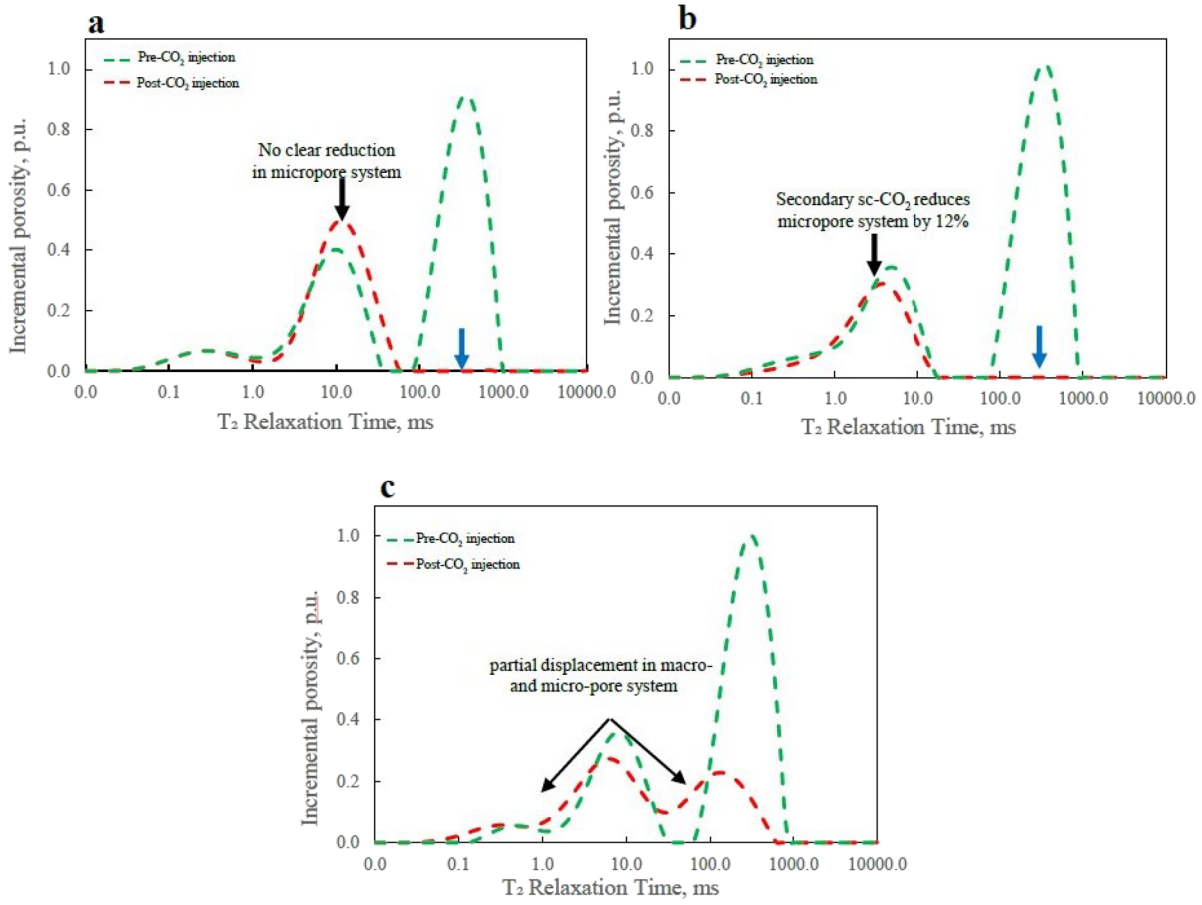

Figure 10. Incremental NMR T_2 of desaturated (green dashed line) and post-CO_2 injection (red dashed line) for composite cores: (a) tertiary miscible CO_2, (b) secondary miscible CO_2 injection, and (c) secondary immiscible CO_2 injection.

Table 9. Summary of NMR T_2 Results for the Three Core-Flood Experiments

composite no.	description	desaturated injection pore volume (cc)	post-CO_2 injection pore volume (cc)	displacement efficiency ED_{NMR} (%)
1	tertiary miscible CO_2 miscible	33	15	55
2	secondary miscible CO_2	33	10	70
3	secondary immiscible CO_2	32	17	47

Table 10. Summary of NMR Displacement Efficiency in Micro- and Macropore Systems for Three Injection Modes

	pore volume pre-CO_2 injection		pore volume post-CO_2 injection	
run no.	micropore system (cc)	macropore system (cc)	micropore system (cc)	macropore system (cc)
1	12.5	20.3	13.6	1.3
2	11.1	21.8	9.8	0
3	10.1	21.8	10.10	7.1

psi, which is insufficient to overcome the high capillary pressure of small pores in tight rocks in addition to the high mobility ratio, resulting in poor displacement.

NMR T_2 measurements confirmed this hypothesis in Figure 12, where a slight reduction in NMR spectra of composite cores was observed (marked with a red brace), indicating limited fluid mobilization in the long T_2 values, which correspond to the macropore system.

In addition, the incremental T_2 profiles of the waterflooding stage were observed to exhibit longer T_2 values than those of the initial desaturated core signals (Figure 13a). This extended T_2 distribution is due to water imbibition, which delays the surface relaxation of the remaining decane and thus leads to longer T_2 distributions (Figure 13b). Clearly, hydrogen communication between micro- and macropore systems aligns with the observation of Anand and Hirasaki.[53]

Tertiary miscible CO_2 injection provided an incremental recovery of 44% OOIP. We speculate that the low incremental recovery is due to increased water content as a result of previous waterflooding. Campbell and Orr[54] stated that water injection prior to CO_2 flooding has a negative impact on pore fluid displacement and oil recovery due to the water film formed during waterflooding, which prevents CO_2 from invading small pores. Given that Scioto has around 1.44 MTMR, this leads to poor displacement efficiency. Although CO_2 has a higher injectivity of 0.01 cc/min/psi than water, an ultimate recovery of approximately 79% OOIP confirms that tertiary miscible CO_2 injection cannot access micropores efficiently (as marked in the black arrow in Figure 10b). Secondary immiscible CO_2 flooding results in an unstable displacement rate of 52%. This is mainly due to the differing densities between the displacing CO_2 gas and the displaced *n*-decane. Poor displacement was observed with a clear fluctuation in the pressure drop during the injection process (Figure 7). Poor displacement was also observed as a

https://doi.org/10.1021/acs.energyfuels.3c03403
Energy Fuels 2023, 37, 19039−19052

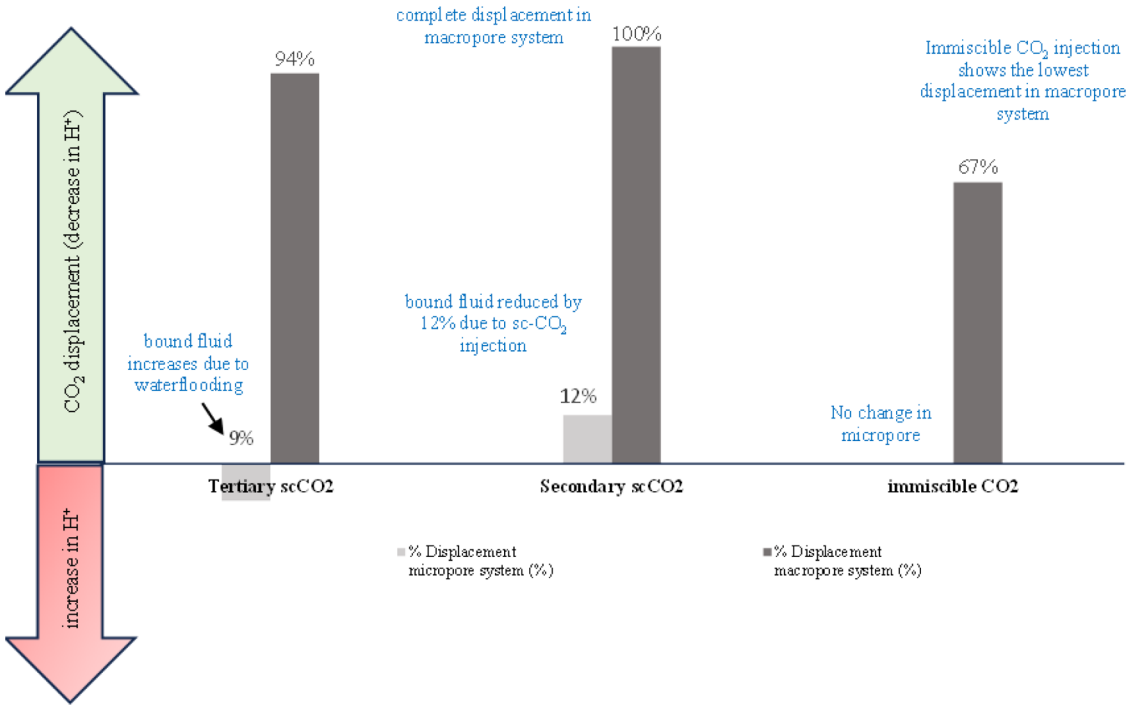

Figure 11. The displacement efficiency of micro- and macropores was determined by NMR analyses.

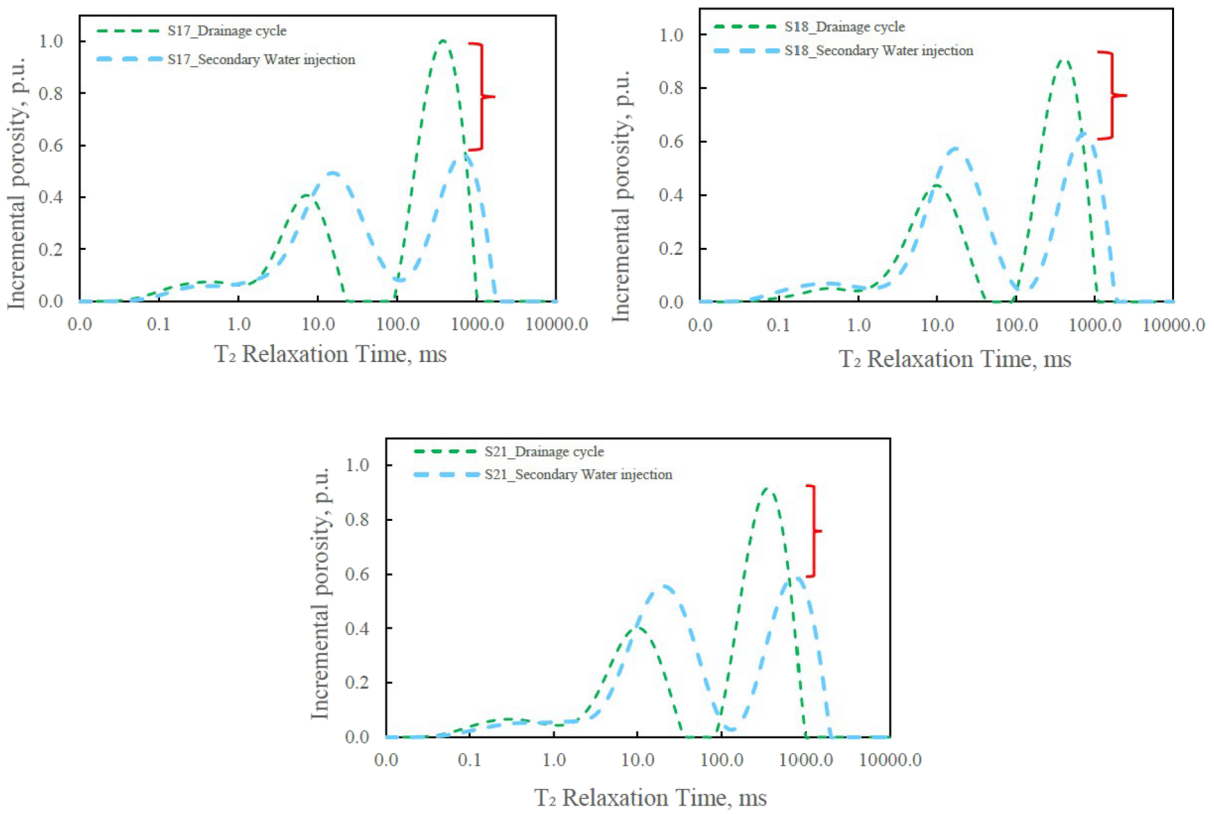

Figure 12. Incremental NMR T_2 curves of desaturated (green dashed line) and waterflooded (light blue dashed line) composite core #1. A slight reduction in the macropore indicates poor displacement as a result of waterflooding (marked in a red brace), while the extended NMR T_2 (light blue dashed lines) is due to the delay of surface relaxation caused by the remaining decane retained in the rock pore system.

partial reduction in the NMR T_2 spectrum compared to the initial desaturated core signal, with an estimated NMR displacement efficiency of about 46% of that of ED_{NMR} (Figure 14). Despite the secondary immiscible CO_2 injection having a high injectivity index of around 0.1 cc/min/psi, the estimated oil recovery reveals a relatively low value of 67% OOIP, which could be attributed to CO_2 gravity override as a consequence of the high-density difference between CO_2 and *n*-decane.[55] In

https://doi.org/10.1021/acs.energyfuels.3c03403
Energy Fuels 2023, 37, 19039−19052

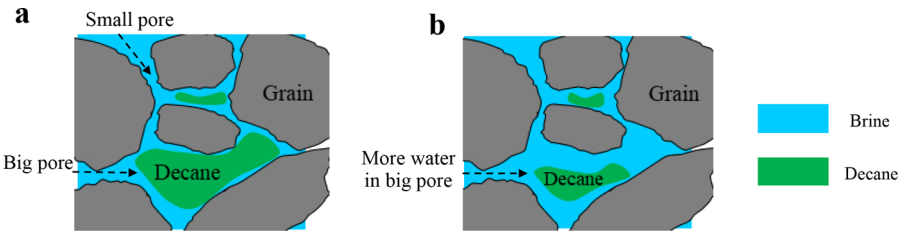

Figure 13. Schematic illustrating the drainage and waterflooding covering. (a) Decane-desaturated case, where decane resides in big pores and water resides in small pores. (b) Waterflooding case shows brine-imbibing big pores causing a slight reduction in decane saturation.

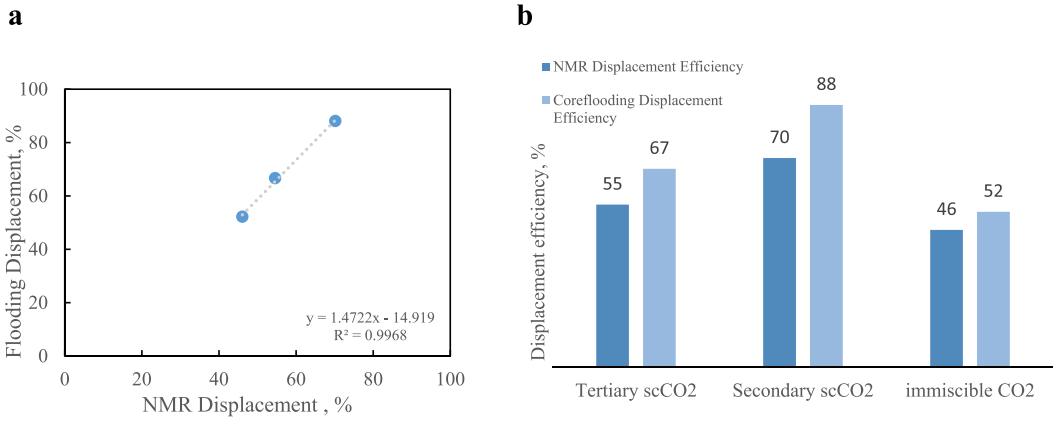

Figure 14. Relation of displacement efficiencies obtained from NMR and core floods using (a) cross-plot and (b) bar chart.

addition, high MTMR could lead to channeling and, thus, a lower displacement efficiency of 52%. Hence, given the low oil recovery and the high gas pore volume injected, we presume immiscible CO_2 injection inefficient EOR method in tight rocks. On the contrary, secondary miscible CO_2 injection shows stable displacement compared to other injection schemes of about 88% E_d. This high efficiency provides the highest recovery factor of approximately 93% OOIP. The high oil recovery is attributed to the stable displacement efficiency due to the miscibility effect that mobilizes fluid from various pore sizes. These findings were aligned with the NMR results, where the NMR displacement efficiency showed about 70% reduction. NMR analysis further revealed that secondary miscible CO_2 injection effectively reduced the macropore signal, indicating decane mobilization from the larger pores (marked with a blue arrow in Figure 10b) in addition to accessing the micropores, as confirmed by the reduction of micropore signal by 12% compared to the desaturated core state (marked with a black arrow in Figure 10b). Based on the comparison of the results obtained, it has been concluded that the secondary miscible CO_2 injection scheme is the most efficient with resident fluid displaced from both micro- and macropore systems, resulting in an oil recovery of 93% OOIP. Displacement efficiency using material balance and NMR for all runs showed a good relation (R^2 = 0.9968, Figure 14).

5. CONCLUSIONS

This study aims to evaluate the efficiency of multiple CO_2 injection schemes in tight sandstone reservoirs. The flooding runs were analyzed in terms of oil recovery, pressure data, injectivity index, and NMR measurements. Based on the findings, the following conclusions are derived:

- Tight Scioto sandstone has bimodal pore throat distributions (micro- and macropore throat systems), as determined by MICP and NMR T_2 results. The SEM results demonstrated that the micropore system is visible with pore-lining illite platelets, indicating a high micropore system capability of 1.44 MTMR.
- Secondary waterflooding provides poor oil recovery and early water breakthrough attributed to multiple factors, including low water injectivity, high capillary forces in small pores, and a high MTMR value. NMR T_2 results confirm poor displacement, as indicated by the extended T_2 spectrum relaxation due to the existence of immobilized decane in the pore system.
- The secondary miscible CO_2 injection provided the highest oil recovery, with approximately 93% OIIP. This was confirmed with the NMR T_2 finding. The miscibility mechanism was able to completely displace the resident fluid in the macropore system in addition to a reduction of around 12% of the micropore system.
- Tertiary miscible CO_2 injection following secondary water flooding depicts an ultimate recovery of around 79% OOIP. Such relatively low recovery performance is due to the increase in water content that retards the micropore CO_2 displacement and hence lowers the injectivity efficiency to ca. 0.01 cc/min/psi. NMR measurements agree with this hypothesis and reveal an increase in hydrogen content in micropores of around 9%, confirming that tiny pores were not accessed by tertiary miscible CO_2 injection.
- Secondary immiscible CO_2 injection provides the least oil recovery of 68% OOIP. The low recovery is due to the displacement instability of 46% ED_{NMR}.
- A significant direct relationship was obtained between the displacement efficiency of core-flood and the NMR T_2 tests, proving that NMR is an effective tool in observing the different pore systems' contribution in overall

https://doi.org/10.1021/acs.energyfuels.3c03403
Energy Fuels 2023, 37, 19039−19052

hydrocarbon recovery and CO_2 storage in tight sandstones.

AUTHOR INFORMATION

Corresponding Authors

Hamad AlKharraa − *Department of Geotechnology, Delft University of Technology, 2628 CN Delft, The Netherlands*; orcid.org/0000-0003-1694-8907; Email: H.S.H.Alkharraa@tudelft.nl

Karl-Heinz Wolf − *Department of Geotechnology, Delft University of Technology, 2628 CN Delft, The Netherlands*; Email: K.H.A.A.Wolf@tudelft.nl

Pacelli Zitha − *Department of Geotechnology, Delft University of Technology, 2628 CN Delft, The Netherlands*; Email: P.L.J.Zitha@tudelft.nl

Authors

Abdulrahman AlQuraishi − *National Centre for Oil & Gas Technology, King Abdulaziz City for Science and Technology, Riyadh 11442, Saudi Arabia*

Ridha Al Abdrabalnabi − *College of Petroleum Engineering and Geosciences, King Fahd University of Petroleum & Minerals, Dhahran 34464, Saudi Arabia*

Mohamed Mahmoud − *College of Petroleum Engineering and Geosciences, King Fahd University of Petroleum & Minerals, Dhahran 34464, Saudi Arabia*; orcid.org/0000-0002-4395-9567

Complete contact information is available at: https://pubs.acs.org/10.1021/acs.energyfuels.3c03403

Author Contributions

H.A.-K.: writing, organization, and experiments. K.-H.W.: supervision, methodology, investigation, and review and editing. M.M.: methodology and data discussion. A.Al.: data investigation and review and editing. P.Z.: supervision, project administration, data discussion, methodology, and review and editing. R.A.A.: experiments and data discussion.

Notes

The authors declare no competing financial interest.

ACKNOWLEDGMENTS

The authors would like to thank Dr. Naif Al Qahtani and Essa Abdullah for their support and insightful conversations in regard to this study. Furthermore, the authors acknowledge the participation of Dr. Hyung Kwak, Mustafa Satrawi, and Jun Gao for their help and support in the NMR measurements. In addition, the authors thank Dr. Abdullah AlMansour, Mohammed AlQarni, Hamdan AlYami, and Hussain Al Ali for their insightful conversations on petrophysical and core-flooding analyses.

REFERENCES

(1) International Energy Agency, 2023. *Oil market report—July 2023*; IEA: Paris, https://www.iea.org/reports/oil-market-report-july-2023.

(2) Lake, L. W. *Enhanced Oil Recovery*; Prentice-Hall: Upper Saddle River, NJ, 1989.

(3) Dake, L. P. *Fundamentals of reservoir engineering*; Elsevier: Amsterdam,1983.

(4) Taber, J. J.; Martin, F. D.; Seright, R. S. EOR screening criteria revisited—Part 1: Introduction to screening criteria and enhanced recovery field projects. *SPE* **1997**, *12* (3), 189−198.

(5) Zitha, P. L. Foam drainage in porous media. *Transport in Porous Media.* **2003**, *52*, 1−16.

(6) Dong, X.; Liu, H.; Chen, Z.; Wu, K.; Lu, N.; Zhang, Q. Enhanced oil recovery techniques for heavy oil and oilsands reservoirs after steam injection. *Applied Energy.* **2019**, *239*, 1190−1211.

(7) Gbadamosi, A. O.; Kiwalabye, J.; Junin, R.; Augustine, A. A review of gas enhanced oil recovery schemes used in the North Sea. *J. Pet. Explor. Prod. Technol.* **2018**, *8*, 1373−1387.

(8) Holditch, S. A. Tight gas sands. *JPT.* **2006**, *58* (6), 86−93.

(9) Economides, M. J.; Nolte, K. G. *Reservoir stimulation*; Prentice Hall: Englewood Cliffs, NJ, 1989.

(10) Osiptsov, A. A. Fluid mechanics of hydraulic fracturing: a review. *JPSE* **2017**, *156*, 513−535.

(11) Taber, J. J.; Seright, R. S. Horizontal injection and production wells for EOR or waterflooding. In *Permian Basin Oil and Gas In SPE Permian Basin Oil and Gas Recovery Conference, Midland, TX*; March 1992. SPE-23952.

(12) Chen, M.; Dai, J.; Liu, X.; Kuang, Y.; Wang, Z.; Gou, S.; Qin, M.; Li, M. Effect of displacement rates on fluid distributions and dynamics during water flooding in tight oil sandstone cores from nuclear magnetic resonance. *JPSE* **2020**, *184*, No. 106588.

(13) Yuan, B.; Wood, D. A. A comprehensive review of formation damage during enhanced oil recovery. *JPSE* **2018**, *167*, 287−299.

(14) Sheng, J. J. Critical review of low-salinity waterflooding. *JPSE* **2014**, *120*, 216−224.

(15) Al Adasani, A.; Bai, B. Analysis of EOR projects and updated screening criteria. *JPSE* **2011**, *79*, 10−24.

(16) Bachu, S.; Adams, J. J. Sequestration of CO_2 in geological media in response to climate change: capacity of deep saline aquifers to sequester CO_2 in solution. *Energy Conversion and management.* **2003**, *44* (20), 3151−3175.

(17) Wang, L.; Wang, S.; Zhang, R.; Wang, C.; Xiong, Y.; Zheng, X.; Li, S.; Jin, K.; Rui, Z. Review of multi-scale and multi-physical simulation technologies for shale and tight gas reservoirs. *J. Nat. Gas Sci. Eng.* **2017**, *37*, 560−578.

(18) Kulkarni, M. M.; Rao, D. N. Experimental investigation of miscible and immiscible Water-Alternating-Gas (WAG) process performance. *JPSE* **2005**, *48* (1−2), 1−20.

(19) Song, Z.; Li, Y.; Song, Y.; Bai, B.; Hou, J.; Song, K.; Jiang, A.; Su, S. A critical review of CO_2 enhanced oil recovery in tight oil reservoirs of North America and China. In *SPE/IATMI Asia Pacific Oil & gas conference and exhibition, Bali, Indonesia*; 2020, October. SPE-196548.

(20) Ali, M.; Jha, N. K.; Pal, N.; Keshavarz, A.; Hoteit, H.; Sarmadivaleh, M. Recent advances in carbon dioxide geological storage, experimental procedures, influencing parameters, and future outlook. *Earth-Science Reviews.* **2022**, *225*, No. 103895.

(21) Holm, L. W.; Josendal, V. A. Mechanism of oil displacement by carbon dioxide. *J. Pet. Technol.* **1974**, *26*, 1427−1438.

(22) Martin, F. D.; Taber, J. J. Carbon dioxide flooding. *J. Pet. Technol.* **1992**, *44* (4), 396−400.

(23) Amao, A. M.; Siddiqui, S.; Menouar, H. A new look at the minimum miscibility pressure (MMP) determination from slim tube measurements. *In the 18th SPE Improved Oil Recovery Symposium, Tulsa, OK*; 14−18 April 2012. SPE 153383.

(24) Sheng, J. J. Critical review of field EOR projects in shale and tight reservoirs. *JPSE* **2017**, *159*, 654−665.

(25) Zuloaga-Molero, P.; Yu, W.; Xu, Y.; Sepehrnoori, K.; Li, B. Simulation study of CO_2-EOR in tight oil reservoirs with complex fracture geometries. *Sci. Rep.* **2016**, *6*, 33445.

(26) Qi, S.; Yu, H.; Xie, F.; Hu, M.; Lu, J.; Wang, Y. Experimental investigation on the CO_2 effective distance and CO_2-EOR storage for tight oil reservoir. *Energy & Fuels.* **2023**, *37* (1), 339−349.

(27) Burley, S.; Worden, R. *Sandston diagenesis: recent and ancient*; Blackwell Publishing Ltd.: Malden, 2003.

(28) Lai, J.; Wang, G.; Wang, Z.; Chen, J.; Pang, X.; Wang, S.; Zhou, Z.; He, Z.; Qin, Z.; Fan, X. A review on pore structure characterization in tight sandstones. *Earth-Science Reviews.* **2018**, *177*, 436−457.

(29) Al Saadi, F.; Wolf, K.; Kruijsdijk, C. V. Characterization of Fontainebleau sandstone: Quartz overgrowth and its impact on pore-throat framework. *J. Pet. Environ. Biotechnol.* **2017**, *7* (328), 1−12.

(30) Xiao, D.; Lu, S.; Yang, J.; Zhang, L.; Li, B. Classifying multiscale pores and investigating their relationship with porosity and permeability in tight sandstone gas reservoirs. *Energy & Fuels.* **2017**, *31* (9), 9188−9200.
(31) Bloch, S.; Lander, R. H.; Bonnell, L. M. Anomalously high porosity and permeability in deeply buried sandstone reservoirs: Origin and predictability. *AAPG Bull.* **2002**, *86*, 301−328.
(32) Salama, A.; Amin, M. F. E.; Kumar, K.; Sun, S. Flow and transport in tight and shale formations: A review. *Geofluids.* **2017**, *2017* (10), 1−21.
(33) Al-Kharra'a, H. S.; Wolf, K. H. A.; AlQuraishi, A. A.; Mahmoud, M. A.; Deshenenkov, I.; AlDuhailan, M. A.; Alarifi, S. A.; AlQahtani, N. B.; Kwak, H. T.; Zitha, P. L. Impact of clay mineralogy on the petrophysical properties of tight sandstones. *Geoen.* **2023**, *227*, No. 211883.
(34) Farid Ibrahim, A.; Nasr-El-Din, H. Evaluation of the breakdown pressure to initiate hydraulic fractures of tight sandstone and shale formations. In *SPE Trinidad and Tobago Section Energy Resources Conference, Trinidad and Tobago*; June 2018. SPE-191245.
(35) Langaas, K.; Ekrann, S.; Ebeltoft, E. A criterion for ordering individuals in a composite core. *J. Pet. Technol.* **1998**, *19* (1−2), 21−32.
(36) Graue, A.; Nesse, K.; Baldwin, B. A.; Spinler, E. A.; Tobola, D. P.; Impact of fracture permeability on oil recovery in moderately water-wet fractured chalk reservoirs. In *SPE Improved Oil Recovery Conference, Tulsa, OK*; April 2002. SPE-75165.
(37) Sakthivel, S.; Abdel-Azeim, S.; AlSaif, B.; Al-Abdrabalnabi, R. Investigating the role of [PF6]− and [BF4]− based ionic liquids for enhanced oil recovery in carbonate reservoirs: Experimental and molecular simulation insights. *J. Mol. Liq.* **2023**, *390*, No. 123006.
(38) Elsharkawy, A. M.; Poettmann, F. H.; Christiansen, R. L. Measuring minimum miscibility pressure: slim-tube or rising-bubble method?. In *SPE Improved Oil Recovery Conference, Tulsa, OK*; 1992, April. SPE-24114.
(39) Ahmed, T. H. Prediction of CO_2 minimum miscibility pressures. In *SPE Latin America and Caribbean Petroleum Engineering Conference, Buenos Aires, Argentina*; 24−27 April, 1994. SPE-27032.
(40) Lias, S. G.; Bartmess, J. E. Gas-Phase Ion Thermochemistry. In *NIST Chemistry WebBook, NIST Standard Reference Data-base Number 69*; Mallard, W. G.; Linstrom, P. J., Eds.; National Institute of Standards and Technology: Gaithersburg, MD, Jan 2000. http://webbook.nist.gov.
(41) Carr, H.; Purcell, E. Effects of diffusion on free precession in nuclear magnetic resonance experiments. *Phys. Rev.* **1954**, *94* (3), 630−638.
(42) Nelson, P. H. Pore-throat sizes in sandstones, tight sandstones, and shales. *AAPG Bulletin.* **2009**, *93* (3), 329−340.
(43) Blunt, M.; Fayers, F. J.; Orr, F. M., Jr. Carbon dioxide in enhanced oil recovery. *Energy conversion and management.* **1993**, *34*, 1197−1204.
(44) Rossen, W. R.; Van Duijn, C. J.; Nguyen, Q. P.; Shen, C.; Vikingstad, A. K. Injection strategies to overcome gravity segregation in simultaneous gas and water injection into homogeneous reservoirs. *SPE J.* **2010**, *15*, 76−90.
(45) Andrianov, A.; Farajzadeh, R.; Nick, M. M., Talanana, M.; Zitha, P. L. Immiscible foam for enhancing oil recovery: bulk and porous media experiments. In *SPE Asia Pacific Enhanced Oil Recovery Conference, Kuala Lumpur, Malaysia*; 19−20 July, 2011. SPE-143578.
(46) Coates, G. R.; Xiao, L.; Prammer, M. G. *NMR logging principles and applications*; Gulf Publishing Company: Houston, TX, 1999.
(47) Mitchell, J. Magnetic resonance core analysis at 0.3 T. In *Proceedings of the International Symposium of the Society of Core Analysts, Avignon, France*; 8−11 September 2014.
(48) Karimi, S.; Saidian, M.; Prasad, M.; Kazemi, H. Reservoir rock characterization using centrifuge and nuclear magnetic resonance: A laboratory study of middle bakken cores. In *SPE Annual Technical Conference and Exhibition*, Houston, TX, USA,28−30 September, 2015. SPE-175069.
(49) Al-Mahrooqi, S. H.; Grattoni, C. A.; Moss, A. K.; Jing, X. D. An investigation of the effect of wettability on NMR characteristics of sandstone rock and fluid systems. *JPSE* **2003**, *39* (3−4), 389−398.
(50) Hassan, A.; Mahmoud, M.; Al-Majed, A.; Al-Nakhli, A. New chemical treatment for permanent removal of condensate banking from different gas reservoirs. *ACS Omega.* **2019**, *4* (26), 22228−22236.
(51) Muqtadir, A.; Elkatatny, S. M.; Mahmoud, M. A.; Abdulraheem, A.; Gomaa, A. Effect of saturating fluid on the geomechanical properties of low permeability Scioto sandstone rocks. In *ARMA US Rock Mechanics/Geomechanics Symposium, Seattle, WA*; 17−20 June, 2018. ARMA-2018−1193.
(52) Juanes, R.; Spiteri, E. J.; Orr, F. M., Jr.; Blunt, M. J. Impact of relative permeability hysteresis on geological CO_2 storage. *Water Resour. Res.* **2006**, *42* (12), W12418 DOI: 10.1029/2005WR004806.
(53) Anand, V.; Hirasaki, G. J. Diffusional coupling between micro and macroporosity for NMR relaxation in sandstones and grainstones1. *Petrophysics* **2007**, *48*, 289−307.
(54) Campbell, B. T.; Orr, F. M. Flow visualization for CO_2/crude-oil displacements. *Society of Petroleum Engineers Journal.* **1985**, *25* (5), 665−678.
(55) Enick, R. M.; Olsen, D. K. *Mobility and Conformance Control for Carbon Dioxide Enhanced Oil Recovery (CO2-EOR) via Thickeners, Foams, and Gels−A Detailed Literature Review of 40 Years of Research*; National Energy Technology Laboratory, DOE/NETL-2012/1540, Activity 4003.200.01; 2012.

https://doi.org/10.1021/acs.energyfuels.3c03403
Energy Fuels 2023, 37, 19039−19052